Inverse Problem of Capillary Filling

Emanuel Elizalde,[1] Raúl Urteaga,[1,*] Roberto R. Koropecki,[1] and Claudio L. A. Berli[2]
[1]IFIS Litoral (UNL-CONICET), 3000 Santa Fe, Argentina
[2]INTEC (UNL-CONICET), 3000 Santa Fe, Argentina
(Received 12 December 2013; published 4 April 2014)

The inverse problem of capillary filling, as defined in this work, consists in determining the capillary radius profile from experimental data of the meniscus position l as a function of time t. This problem is central in diverse applications, such as the characterization of nanopore arrays or the design of passive transport in microfluidics; it is mathematically ill posed and has multiple solutions; i.e., capillaries with different geometries may produce the same imbibition kinematics. Here a suitable approach is proposed to solve this problem, which is based on measuring the imbibition kinematics in both tube directions. Capillary filling experiments to validate the calculation were made in a wide range of length scales: glass capillaries with a radius of around 150 μm and anodized alumina membranes with a pores radius of around 30 nm were used. The proposed method was successful in identifying the radius profile in both systems. Fundamental aspects also emerge in this study, notably the fact that the $l(t) \propto t^{1/2}$ kinematics (Lucas-Washburn relation) is not exclusive of uniform cross-sectional capillaries.

DOI: 10.1103/PhysRevLett.112.134502 PACS numbers: 47.85.-g, 02.30.Zz, 47.55.nb

Though capillary-driven imbibition of micro- and nanotubes has been well documented over the past century [1], the topic is experiencing a renaissance at present. This is because capillarity phenomena enter a wide variety of systems that range from living organisms to lab-on-a-chip devices. Several fundamental and practical aspects of the phenomena are currently being discussed in the literature, such as the effects of inertia [2,3], wall roughness [4], contact angle [5], and strong confinements [6]. In particular, here we deal with the capillary filling of tubes with nonuniform cross sections, in the fluid dynamic regime where the fluid kinematics is controlled by viscous dissipation [2,3]. Thus, if inertial and gravity effects are neglected, the meniscus velocity $u = dl/dt$, where l is the meniscus position and t is time, is given by

$$u(l) = \frac{\gamma \cos(\theta)}{4\mu r(l)^3 \int_0^l r(x)^{-4} dx}. \quad (1)$$

In this expression, x is the axial coordinate along the tube, $r(x)$ is the axially dependent tube radius, μ is the fluid dynamic viscosity, γ is the air-liquid surface tension, and θ is the equilibrium contact angle made by the liquid with the solid. The case of ideal surfaces is considered, with smooth radius variations and homogeneous properties along the tube, so that the variation of the contact angle is negligible in relation to the equilibrium one. Equation (1) derives from the balance between the Laplace driving force and the viscous resistance in capillaries of a circular cross section, and it has been used by several authors to predict the instantaneous position of the meniscus, given a function $r(x)$ specified beforehand [7–10]. That procedure may be designated a direct, or forward, calculation. In fact, in the context of Eq. (1), the inverse problem consists in determining a completely unknown function $r(x)$ from the curve of experimental data $u(x)$. This possibility has not been discussed in the literature before, and it is the objective of the present work.

It is worth noting here that extracting $r(x)$ from Eq. (1) is an ill-posed problem, meaning that it has multiple solutions. This may appear rather trivial from the viewpoint of mathematics; however, it represents a novelty in the physics of fluids: capillaries with different geometries may have the same $l(t)$ curve, including the well-known relation $l(t) \propto t^{1/2}$, i.e., Lucas-Washburn (LW) result [11,12], which has been invariably associated with uniform capillaries. Apart from the fundamental aspect, solving the inverse problem of Eq. (1) involves several potential applications, for example, in the design of capillary pumps for microfluidic systems, where the liquid handling is encoded in the geometric design of microchannels [13]. On the other hand, determining $r(x)$ from the kinematics of capillary filling offers the possibility to characterize the inner geometry of nanopores in a nondestructive manner (the detailed internal structure of nanochannels is still inaccessible to ordinary techniques used in nanotechnology laboratories). This is of great interest in the case of nanoporous substrates, which are produced for a number of applications, for instance, in optofluidic microsystems [14]. In any case, solving the inverse problem of Eq. (1) presents several difficulties, as we discuss below.

Equation (1) can be converted into a differential equation by using the Leibnitz rule, which yields

$$\frac{d}{dl}[r(l)u(l)^{1/3}] = -\frac{4u(l)^{4/3}}{3\alpha}, \quad (2)$$

where $\alpha = \gamma\cos(\theta)/\mu$ is a coefficient that characterizes fluid properties, and can be assumed as a constant for a given temperature. Integrating Eq. (2) leads to an explicit expression of the unknown function $r(l)$,

$$r(l) = [r(l_0)u(l_0)^{1/3} + \frac{4}{3\alpha}\int_l^{l_0} u(l)^{4/3}dl]u(l)^{-1/3}, \quad (3)$$

where l_0 is an arbitrary limit of integration. The multiplicity of solutions of Eq. (3) is illustrated in Fig. 1. If one introduces $u(l)$ as the meniscus velocity corresponding to a cylindrical capillary of radius R, that is, from the curve $l(t)$ corresponding to the LW result [Fig. 1(a)], then Eq. (3) yields an infinite family of curves $r(x)$ parametrized by $r(l_0)$, as shown in Fig. 1(b).

From the physical point of view, a remarkable feature here is that any of the tube profiles $r(x)$ plotted in Fig. 1(b), when imbibed by capillary action, produce the curve $l(t)$ plotted in Fig. 1(a), which in this example corresponds to the LW dynamics for cylindrical tubes. It means that, in doing the direct calculation with Eq. (1), there are several capillary geometries that produce the same meniscus velocity $u(l)$.

Concerning the inverse problem, it is evident that identifying the right $r(x)$ solution among the parametrized family of curves demands additional information from the problem. One needs to know $r(l_0)$ or any single datum other than the curve $u(l)$, for example, the total tube volume. Previous knowledge of symmetric variations of the tube profile is also useful for this purpose. Actually, in Eq. (3), $r(l_0)$ is the boundary condition required to confer uniqueness to the solution. In this regard, choosing $l_0 = L$ is the most appropriate option to compute the integral in Eq. (3), provided the ending radius $r(L)$ could be measured. Nevertheless, this calculation procedure propagates the inaccuracy of $r(L)$ to the entire solution $r(x)$.

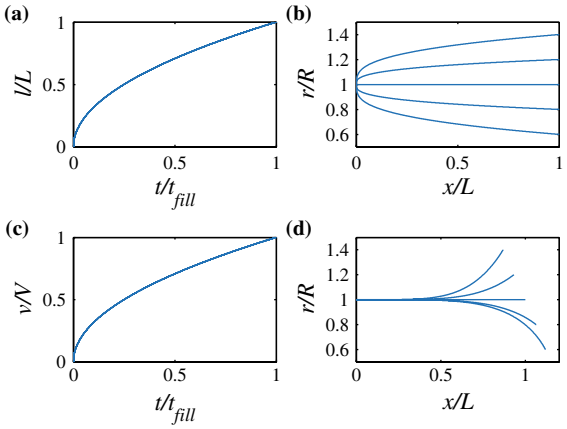

FIG. 1 (color online). (a) Relative meniscus position as a function of normalized time for a capillary tube of uniform radius R and length L; $t_{\text{fill}} = 2L^2/(\alpha R)$ is the filling time. (b) Functions $r(x)$ obtained from Eq. (3) with $u(l)$ calculated from data $l(t)$ on the left, for different values of $r(l_0)$. (c) Fluid volume fraction related to the meniscus position as a function of normalized time for a capillary tube of uniform radius R and length L. (d) Functions $r(x)$ obtained from Eq. (4) with $Q(v)$ calculated from data $v(t)$ on the left, for different values of $r(v_0)$.

Alternatively, here we propose a different strategy that avoids the necessity of knowing the radius at any position. It takes advantage of the possibility to measure capillary filling in both tube directions: from $x = 0$ to L, and from $x = L$ to 0. The second measurement, when processed through Eq. (3), generates a new family of $r(x)$ curves, where one of them must reproduce the meniscus velocity of the first measurement. Thus, the procedure allows one to identify the right function $r(x)$ that represents the tube geometry. It is worth adding that, since this method produces two solutions, the inverse problem is now overdetermined. Nevertheless, cross-checking the two independent solutions also serves as a consistency test for the model.

In order to validate this approach, experiments of capillary filling were made in a wide range of length scales. Two different systems were used: a glass capillary of radius around 150 μm and an anodized alumina membrane with straight, noninterconnected, monodisperse pores of radius around 30 nm, with both ends open to the atmosphere. In the first case, the radius profile $r(x)$ can be readily determined by optical methods, which is useful to contrast with theoretical calculations. In the second case, $r(x)$ is unknown and the experiment serves to demonstrate the method utility.

Next, the solution of the inverse problem in the glass capillary is discussed. The nonuniform cross-sectional tube was fabricated in our lab by heating and pulling a glass capillary. Neither the load at the capillary end nor the local heating were uniform, so as to produce a smooth variation of the tube radius along the capillary [Fig. 2(b)]. The resulting radius profile was determined by photography image analysis [Fig. 2(d), black curve]. A glycerol–2-propanol mixture was employed, with the viscosity tuned to fill the 5 cm length capillary in about 10 min. The meniscus position was followed by using a CCD camera [9,15,16]; images were recorded at the rate of three pictures per second. Before each run, the capillary was systematically washed with water, acetone, and 2-propanol, and then dried in an oven. Experiments were made at room temperature. The time variations of the meniscus position obtained in typical runs are plotted in Fig. 2(c).

In the following we will use the red color to identify the filling process in the left-to-right direction [red curve in Fig. 2(c)] and the blue color to the filling process in the opposite direction [dashed blue curve in Fig. 2(c)]. The velocities $u(l)$ in both directions were obtained by numerical differentiation of the curves l versus t using local quadratic regression. Taking $u(l)$ from the red data, and using Eq. (3) with arbitrary $r(L)$ values, yields a family of possible solutions for $r(x)$. With these functions, the

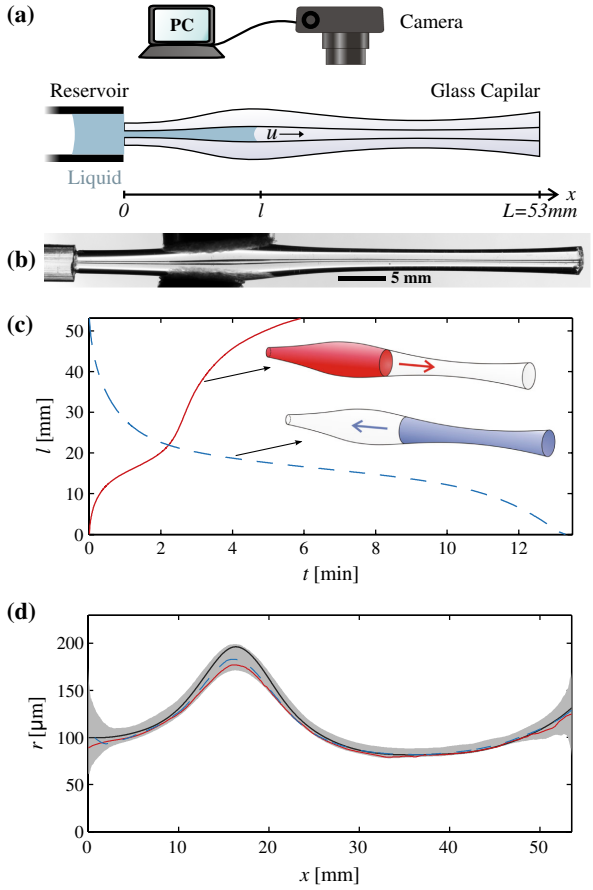

FIG. 2 (color online). (a) Experimental setup to measure the filling dynamics of a glass capillary, including a scheme of the capillary with the imbibing fluid, and the coordinate systems used in calculations. (b) Picture of the nonuniform cross-sectional glass capillary. (c) Meniscus position as a function of time measured from $x = 0$ to L (continuous red) and from $x = L$ to 0 (dashed blue). (d) Capillary radius as a function of the axial distance. The black curve is the measured profile determined by photography image analysis. The continuous red curve and the dashed blue curve are the predicted $r(x)$ functions. The shaded area represents the confidence bounds obtained from different trials.

expected blue filling data are simulated by using Eq. (1). The simulated l versus t curves are compared to the measured blue curve, to identify the right $r(x)$ function by the minimum least-squares fit. The $r(x)$ solution thus obtained is plotted in Fig. 2(d) (red curve). The whole procedure is then repeated starting with the blue l versus t curve [Fig. 2(c)], which produces the blue $r(x)$ curve in Fig. 2(d). All calculations were made by using $\alpha = 0.18$ m. The shaded area in Fig. 2(d) was obtained by propagating the uncertainties of the experimental data from five measurements in each direction, by using Monte Carlo simulations of synthetic data sets [17].

It is relevant to note that the overlapping of the two obtained solutions shows the consistency of the calculation procedure. Furthermore, the close agreement of these solutions with the experimentally measured $r(x)$ data [black curve, Fig. 2(d)] indicates that the fluid dynamic model used is appropriate.

The imbibition process can be experimentally assessed by using other techniques, apart from the one described above to capture the instantaneous position of the meniscus. In fact, particularly for nanoporous matrices, it is usual to measure the amount of imbibed fluid as a function of time by using gravimetric methods [18], neutron absorption [19], reflected light interference [10,20], or simply by geometric measurement of the imbibed volume [21]. To take into account these possibilities, we extend the model to the case where experimental data are proportional to the volume of imbibed fluid $v(l)$. Introducing $dv(x) = \pi r(x)^2 dx$ into Eq. (1) and reproducing the procedure to derive Eq. (3) yields

$$r(v) = \left[r(v_0)^5 Q(v_0)^5 + \frac{20}{\alpha\pi^2} \int_v^{v_0} Q(v)^6 dv \right]^{1/5} Q(v)^{-1}, \tag{4}$$

where $Q = dv/dt$ is the volume flow rate. It is worth noting that this change of variables does not avoid the ill-posed nature of the problem. The multiplicity of solutions of Eq. (4) is illustrated in Fig. 1(d). In this figure, the parametrized curves $r(x)$ involve different tube lengths, as they correspond to the same capillary volume V.

Next, the solution of the inverse problem in the anodized alumina membrane is discussed. The nanoporous membrane was fabricated by the two-step anodization process described elsewhere [10,22]. The membrane surfaces were inspected by SEM, and a typical image is included in Fig. 3(a). The measured interpore distance d_i was around 101 ± 1 nm, and pore radii were estimated to be around 34 ± 5 and 28 ± 5 nm, for each side of the membrane, respectively (SEM image analysis). The membrane thickness was $L = 75$ μm, as obtained by optical microscopy. Capillary filling measurements were carried out by using the experimental setup reported in previous works [10,20]. Between runs the membrane was washed with 2-propanol and dried at room temperature. Reflected light intensity as a function of time is measured after a liquid drop (2-propanol) impinges over the membrane, as shown in Fig. 3(a). The sensed light intensity is the result of the interference of light reflected from the two fixed interfaces [10,20]. The oscillations in reflectance [inset in Fig. 3(b)] are a consequence of constructive and destructive interference when the effective optical thickness of the membrane is increased by the liquid intake. With a simple model of effective medium, the extreme positions are converted into the imbibed fluid volume fraction v/V [Fig. 3(b)]. Additionally, the total number of extremes N and the membrane thickness L can be used to obtain the membrane porosity, $P \approx 34\%$ [10,20].

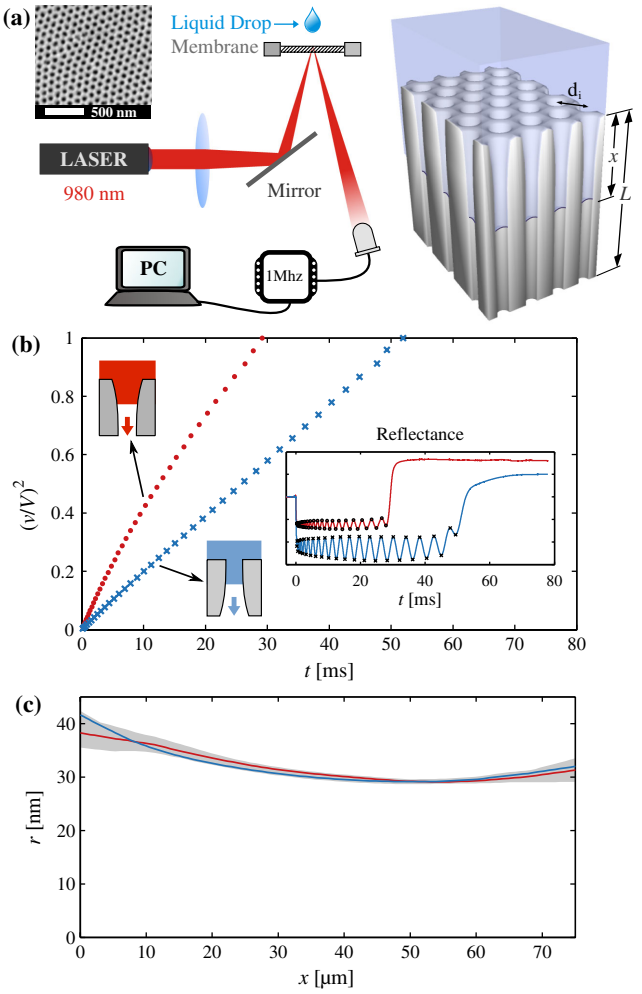

FIG. 3 (color online). (a) Diagram of the experimental setup including a SEM image of the membrane and a schematic representation of the nanochannel array with the imbibing fluid and the coordinate systems used in calculations. (b) Square volume fraction of the imbibed fluid as a function of time, obtained from the extremes of the reflectance oscillations (inset), measured from different sides of the membrane. (c) Capillary radius as a function of the axial distance. The continuous red curve and the dashed blue curve are the predicted $r(x)$ functions. The shaded area represents the confidence bounds obtained from five different trials in each direction.

Given the well-ordered array of pores in anodized alumina [Fig. 3(a)], the membrane is regarded as an assembly of straight nanochannels aligned in the flow direction, all of them with the same length and pore radius profile [22]. Thus, the velocity at which the liquid invades the membrane is that of the capillary-driven flow in each single pore, and hence the single capillary model can be used to interpret the filling dynamics of the whole membrane. To determine the membrane pore radius profile, a procedure analogous to that used above for the glass capillary is followed. The measured volume fraction v/V was numerically differentiated by central differences to obtain $Q(v)/V$. The solutions for measurements in each direction [red and blue data, Fig. 3(b)] were obtained using Eq. (4), and they are reported in Fig. 3(c). The radii as a function of volume are converted into radii as a function of position with $dv(x) = \pi r(x)^2 dx$. Absolute values of the radius profile were obtained by using the experimental value of L and the tabulated properties of 2-propanol at 20 °C.

The solutions $r(x)$ obtained [red and blue data, Fig. 3(c)] coincide within the shaded area that represents the error. This agreement shows the consistency of the method. Moreover, the radius values at the pore ends are in agreement with those obtained from SEM image analysis in both membrane faces. Additionally, the membrane porosity estimated with the results in Fig. 3(c) and the interpore distance is $P = 36\%$, which coincides with the porosity obtained from the total number of extremes N. These results confirm that the solution of the inverse problem proposed here is suitable to determine the pore radius profile in a wide range of length scales. The method is also self-sufficient in the sense that no additional data are needed to identify the right solution.

In conclusion, one may observe that the present work contributes to elucidate two main aspects of capillary filling. First, the ill-posed problem related to the inversion of Eq. (1) is revealed. The physical consequences of this mathematical feature are remarkable, namely, the fact that capillaries with different radius profiles may present the same filling dynamics. The second relevant aspect concerns the attractive applications of the method proposed to solve the inverse problem. In fact, the possibility to accurately identify the internal geometry of nanochannels in a nondestructive manner is of particular interest for the characterization of nanoporous matrices. In addition, both the model and the calculation procedure are useful to rationalize the design of passive microfluidic pumps, where the liquid transport is controlled by the geometry of micro- and nanochannels. In microfluidic systems, however, rectangular cross-section channels having sharp corners pose several problems to model capillary-driven transport, due to the particular effect of edges. Additionally, the hydrodynamic resistance involves two possible dimensional variations (width and/or depth, as a function of axial distance). Handling these difficulties in modeling is precisely one of our research interests at present.

The authors acknowledge financial support from the CONICET and the Universidad Nacional del Litoral, Argentina. The technical assistance of H. Arias and J. Sanpietro is also acknowledged.

*urteagar@santafe-conicet.gov.ar

[1] P.-G. de Gennes, F. Brochard-Wyart, and D. Quéré, *Capillarity and Wetting Phenomena: Drops, Bubbles, Pearls, Waves* (Springer, New York, 2004).

[2] N. Fries and M. Dreyer, J. Colloid Interface Sci. **327**, 125 (2008).
[3] S. Das and S. K. Mitra, Phys. Rev. E **87**, 063005 (2013).
[4] D. Geromichalos, F. Mugele, and S. Herminghaus, Phys. Rev. Lett. **89**, 104503 (2002).
[5] M. Popescu, J. Ralston, and R. Sedev, Langmuir **24**, 12710 (2008).
[6] J. Haneveld, N. Tas, N. Brunets, H. Jansen, and M. Elwenspoek, J. Appl. Phys. **104**, 014309 (2008).
[7] D. Erickson, D. Li, and C. Park, J. Colloid Interface Sci. **250**, 422 (2002).
[8] W. Liou, Y. Peng, and P. Parker, J. Colloid Interface Sci. **333**, 389 (2009).
[9] M. Reyssat, L. Courbin, E. Reyssat, and H. Stone, J. Fluid Mech. **615**, 335 (2008).
[10] R. Urteaga, L. Acquaroli, R. Koropecki, A. Santos, M. Alba, J. Pallares, L. Marsal, and C. Berli, Langmuir **29**, 2784 (2013).
[11] R. Lucas, Kolloid Z. **23**, 15 (1918).
[12] E. Washburn, Phys. Rev. **17**, 273 (1921).
[13] M. Zimmermann, H. Schmid, P. Hunziker, and E. Delamarche, Lab Chip **7**, 119 (2007).
[14] X. Fan and I. White, Nat. Photonics **5**, 591 (2011).
[15] W. Holloway, J. Aristoff, and H. Stone, Phys. Fluids **23**, 081701 (2011).
[16] S. Girardo, S. Palpacelli, A. De Maio, R. Cingolani, S. Succi, and D. Pisignano, Langmuir **28**, 2596 (2012).
[17] S. A. Teukolsky, W. T. Vetterling, B. P. Flannery, and W. H. Press, *Numerical Recipes: The Art of Scientific Computing* (Cambridge University Press, Cambridge, England, 2007).
[18] S. Gruener and P. Huber, Phys. Rev. Lett. **103**, 174501 (2009).
[19] S. Gruener, Z. Sadjadi, H. Hermes, A. Kityk, K. Knorr, S. Egelhaaf, H. Rieger, and P. Huber, Proc. Natl. Acad. Sci. U.S.A. **109**, 10245 (2012).
[20] L. Acquaroli, R. Urteaga, C. Berli, and R. Koropecki, Langmuir **27**, 2067 (2011).
[21] C. Grzelakowski, D. Jazia, B. Lebeau, L. Vonna, D. Dupuis, and H. Haidara, Langmuir **25**, 5855 (2009).
[22] K. Nielsch, J. Choi, K. Schwirn, R. B.Wehrspohn, and U. Gösele, Nano Lett. **2**, 677 (2002).